Radiation characteristics of a high-frequency antenna in different dielectric environments

Radiation characteristics of a high-frequency antenna in different dielectric environments

C. Warren
Edinburgh Napier University
School of Engineering & the Built Environment
Merchiston Campus, Edinburgh, EH10 5DT, UK
C.Warren@napier.ac.uk

N. Chiwaridzo, A. Giannopoulos
University of Edinburgh
Institute for Infrastructure & Environment
School of Engineering
The King's Buildings, Edinburgh, EH9 3JL, UK
s0970494@ed-alumni.net, A.Giannopoulos@ed.ac.uk

***Abstract*—This paper presents an investigation of the radiation characteristics and sensitivity of a high-frequency Ground-Penetrating Radar (GPR) antenna using radiation patterns obtained from both physical measurements and a three-dimensional (3D) Finite-Difference Time-Domain (FDTD) numerical model. The aim was to develop an understanding of how electromagnetic energy is radiated and received by a real GPR antenna in lossy dielectric environments. The radiation patterns were obtained by measuring responses from a target positioned at a series of intervals on the circumference of a circle surrounding the antenna in the H-plane. We believe this approach offers a more realistic characterisation of antenna behaviour and is therefore a useful addition to the traditional transmitted field pattern. Measured patterns came from a 1.5 GHz commercial antenna. A series of oil-in-water emulsions were used to simulate homogeneous materials with different permittivities ($\epsilon_r = 5, 10, 30, 72$) and with frequency-dependent conductivities. The measured patterns were compared with modelled ones obtained from a 3D FDTD model which included a description of the antenna. Good correllation was shown between the experimental results and modelled data with respect to the strength of the main lobe within the critical angle window. However, there are discrepancies in the strength of main lobe at shallow angles. In all the dielectrics the main lobes are generally broad due to the near-field observation distance but, as expected, become narrower with increasing permittivity. Using the FDTD model, further research is planned to compare these received energy patterns with transmitted field ones.**

***Index Terms*—Antennas, radiation patterns, experiments, FDTD**

I. Introduction

Ground-Penetrating Radar (GPR) is used in a wide range of different applications in the fields of engineering and geophysics. The diversity of GPR usage has meant there are a number of different GPR antenna designs available commercially, and also used within the academic community for research. The type and size of a GPR antenna is usually dependent on the application, e.g. low frequency antennas, which are physically larger, are used where significant depth of penetration is important, whereas high frequency antennas, which are physically smaller, are used where less penetration and better resolution are required. Understanding how energy is transmitted and received by a particular GPR antenna has many benefits: it could lead to more informed usage of the antenna in GPR surveys; improvements in antenna design; and better interpretation of GPR signal returns from the ground/structure. The radiation characteristics of a particular antenna are usually investigated by studying the radiation patterns and directivity. For GPR antennas it is also important to study these characteristics when the antenna is in different environments that would typically be encountered in GPR surveys.

Studies of antenna radiation characteristics can be divided into three areas: theoretical analysis, measured data, and numerical modelling. The theoretical radiation patterns of simple antennas, such as the cylindrical monopole, can be completely predicted in free-space [1]. Another example is the infinitesimal dipole which in free-space exhibits two-dimensional (2D) patterns that are sections of the classic torus shape. There are also theoretical approximations for the far-field patterns of infinitesimal dipole antennas over lossless [2] and low-loss [3] half-spaces.

The radiation pattern of one antenna can be measured directly with a second antenna, and this has been done in free-space for simple antennas as well as for more widely-used commercial GPR antennas [4]–[6]. There are also laboratory measurements of radiation patterns of simple antennas over homogeneous materials obtained directly with another antenna [7], and indirectly through the recording of responses from a simple target [6], [8]. Measuring antenna radiation patterns in free-space requires an antenna range with accurate positioning equipment, and the outcome is of limited use for GPR. To directly measure antenna radiation patterns in realistic materials, which is useful for GPR, presents many practical difficulties. This has prompted numerical simulations of GPR antenna radiation patterns.

The state of numerically derived GPR antenna radiation patterns is similar to that of measured data, and reflects the state of GPR antenna modelling in general. Radiation patterns of simple and more complex antennas have been modelled in free-space, but only radiation patterns of simple antennas have been modelled over realistic materials. A good summary of the current state of theoretical versus measured versus modelled radiation patterns of infinitesimal dipoles located over lossless and low-loss half-spaces is provided by [9].

This paper presents an investigation of the radiation characteristics of a high-frequency GPR antenna, using modelled and measured data, over a range of different lossy dielectrics.

The paper begins by describing the apparatus and experimental procedure that was used to measure data from the 1.5 GHz commercial GPR antenna. Emulsions were used to simulate materials with different permittivities and conductivities. Next, the Finite-Difference Time-Domain (FDTD) antenna model that was developed and used to create numerical radiation patterns is described. The antenna model replicates all the detailed geometry and main components of the real antenna. Finally, the paper focuses on comparing the measured and modelled patterns, and using them to analyse the radiation characteristics of the antenna.

II. Experimental Procedure

A series of experiments were conducted to characterise the radiation dynamics and sensitivity of a commonly used high-frequency GPR antenna – a Geophysical Survey Systems, Inc. (GSSI) 1.5 GHz antenna – in different dielectric environments. A series of oil-in-water (O/W) emulsions were used to simulate materials with different electric properties. As well as being able to control the permittivity and conductivity of the emulsions, there was a practical advantage of being able to easily position targets in them. Details of the design and chemistry of the emulsions can be found in [10]. Three emulsions were used with relative permittivities of 5, 10, and 30. In addition, tap water with relative permittivity 72 provided a fourth dielectric environment.

The main components of the experimental apparatus were: a 50L galvanised steel tank; a plastic rig to mount and position the antenna and target; and a high-shear batch mixer and plastic mixing vessel; and the GPR system and antenna. A 12 mm steel rebar was used as a target to measure the back-scattered response from, and hence investigate the radiation characteristics of the antenna. The rebar could be positioned at 6° increments on a circle of radius 110 mm (centre taken as the mid-point between the transmitting (T_x) and receiving (R_x) elements of the antenna).

The first step of the experimental procedure was to mix the emulsion to be used in the test until it became a visually homogeneous medium. Previous research by [10] had shown that mixing the emulsion continually for a period of 15 minutes using the high-shear batch mixture would ensure it would be stable for several days (sufficient for the 1-2 hours duration of the experiment). The permittivity of the emulsion was then checked by recording responses from an empty tank with the tank base adjusted to two different height positions. Knowledge of the internal antenna geometry and the tank dimensions meant a theoretical path distance could be calculated. Combined with the time difference between the two responses recorded by the GPR system, a velocity and hence permittivity for each emulsion was calculated. This was checked against the designed permittivity value for each emulsion. This indirect method was used to measure the permittivity as there was no equipment available to measure permittivity directly. At the end of each series of measurements the permittivity was checked to ensure it was remaining stable.

Measurements to characterise the radiation dynamics and sensitivity of the antenna began by placing the antenna on the surface of the liquid and recording a response from the empty tank. This reading was used for background removal in subsequent measurements that included the target. The rebar was then inserted into each of the holes in the plastic rig in turn. At each position the response was recorded for approximately 10 seconds duration. This experimental procedure was repeated for the three emulsions and water.

III. Finite-Difference Time-Domain antenna model

The numerical antenna model is representative of a typical high-frequency, high-resolution GPR antenna primarily used for the evaluation of structural features in concrete: the location of rebar, conduits, and post-tensioned cables, as well as the estimation of material thickness on bridge decks and pavements.

Planar bowties are used for the T_x and R_x elements of the antenna. The bowties have a flare angle of 76° and additional rectangular patches added to their open ends. These extensions perform like straight sections of waveguide, which introduce a delay in the signal path and create destructive interference patterns that reduce unwanted resonance. The bowties are etched from copper onto the Printed Circuit Boards (PCB), and enclosed in a rectangular metal boxes which shields the antenna. An open-cell carbon-loaded foam which acts as a ultra-wideband (UWB) electromagnetic absorber to reduce unwanted resonance is used in the cavities behind the bowties. Generally, carbon-loaded UWB microwave absorbers, e.g. Emerson and Cuming ECCOSORB LS (http://www.eccosorb.com), have a permeability of 1 but can have permittivities ranging from 1.25–30.

The excitation of the antenna — pulse shape, frequency content, and feed method — is important for the performance of the real antenna, and hence critical to capture in the model. In common with many other GPR simulations [11]–[14] a Gaussian shaped pulse was assumed with a centre frequency close to the manufacturers specification. Although a simple Gaussian shape is a good approximation, it may not be an entirely realistic representation of the real pulse shape. A simple feed model consisting of a voltage source with internal resistance inserted in a one-cell gap between the two arms of the transmitter bowtie (the drive-point) was used. The receiver circuitry was modelled as a lumped resistance using a cell edge with specific conductance inserted in a one-cell gap between the two arms of the receiver bowtie.

All of the simulations conducted for this research used GprMax3D which is part of GprMax, a suite of electromagnetic wave simulators based on the FDTD method. GprMax (http://www.gprmax.org/) is freely available software that was written by [15] originally in 1996, and has since developed into a mature application that has been successfully used by a number of researchers [16]–[19]. A GprMax3D input file for the antenna model was created from an analysis of the geometry and main components of a real GPR antenna, along with an optimisation process for determining unknown

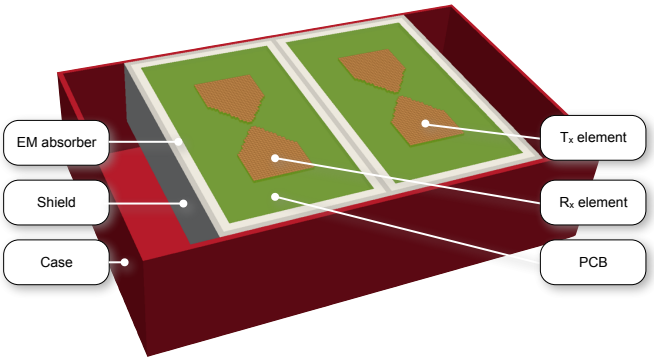

Fig. 1. FDTD mesh of geometry of a GSSI 1.5 GHz antenna

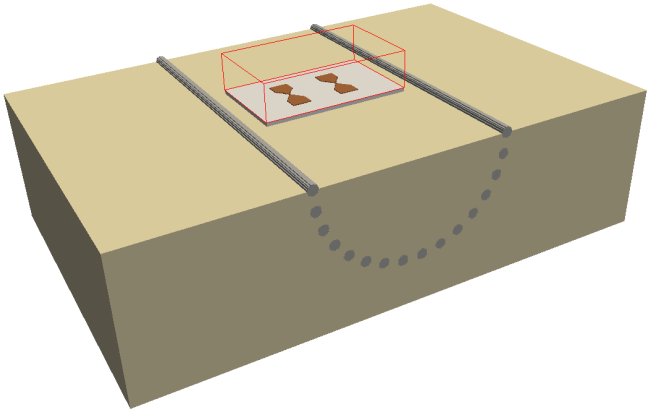

Fig. 2. FDTD mesh of experimental apparatus (only a selection of rebar positions are shown, and the tank and some details of the antenna are omitted for clarity of illustration.)

parameters. Details of the antenna model development and the subsequent validation can be found in [10]. Fig. 1 shows the detailed FDTD mesh of the geometry of the antenna, and Fig. 2 shows the FDTD mesh of the experimental apparatus. A spatial discretisation of $\Delta x = \Delta y = \Delta z = 1$ mm was chosen as a good compromise between accuracy and computational requirements. GprMax computes the spatial and temporal derivatives using a standard second-order scheme and this choice of spatial discretisation also ensured that any numerical dispersion was adequately controlled. The Courant Friedrichs Lewy (CFL) condition was enforced which resulted in a time-step of Δt = 1.926 ps.

The three emulsions used in the experiments have frequency-dependent conductivities [10] which were modelled by fitting a Debye formulation [22]. The conductivity profiles of the emulsions and the tap water (also modelled as a Debye medium) are shown in Fig. 3 over frequencies of interest for high-frequency UWB GPR antennas.

IV. Experimental and Modelled Radiation Patterns

Before the results from the experiments and numerical models are presented the process used to calculate the radiation

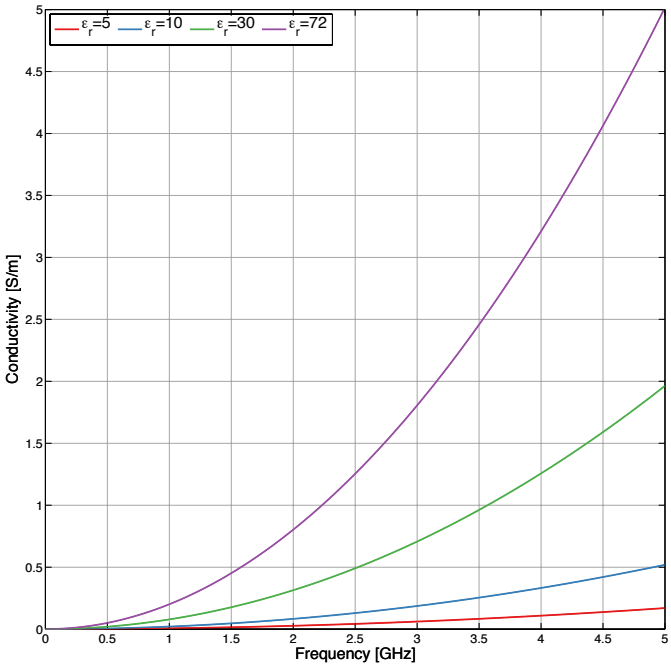

Fig. 3. Frequency dependent conductivity profiles of the emulsions and tap water

patterns is described. Traditionally antenna patterns are plotted at a single frequency, however this is not representative of the behaviour of an impulse-driven UWB GPR antenna. The following process was used to calculate both the experimental and modelled radiation patterns for the antenna in the different dielectric environments. Firstly, for each rebar position a background response (from the empty tank) was subtracted from the recorded A-scan (for the experimental data, an averaged A-scan was taken from several seconds of measurements). Then a measure of the received energy from the rebar wavelet was taken using Eq. (1) proposed by [20]. It is a measure of the energy at the observation radius and angular position.

$$E_T(r,\theta) = \sum \frac{E(r,\theta)^2}{Z} \tag{1}$$

E_T is the total energy at a given radius (r) and angle (θ); E is the electric field value at a given radius (r) and angle (θ); and Z is the electromagnetic impedance of the medium. It was found that this metric produced similar results to picking the maximum positive peak from the rebar wavelet.

In all our results only H-plane radiation patterns are plotted because: firstly, a H-plane pattern is of most interest for GPR as it is usually parallel to the survey direction; and secondly, only H-plane patterns were obtained from the experimental work. The back lobe, i.e. the part in air, of the pattern has been omitted from the plots. This is because a measure of the energy from the rebar wavelet in air was difficult to reliably obtain from the experimental data. Where experimental and modelled patterns are plotted together, each pattern has been normalised to allow a direct comparison. All patterns are plotted on a logarithmic scale unless otherwise stated. The

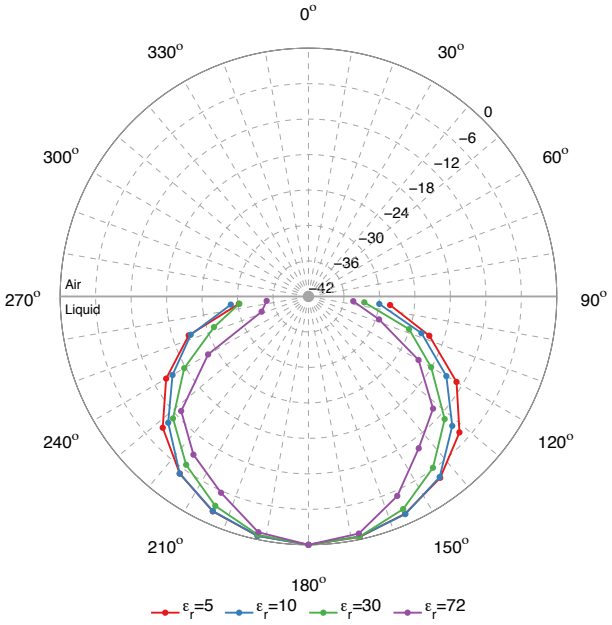

Fig. 4. Experimental 'received energy' H-plane patterns in all dielectric environments ($\epsilon_r = 5, 10, 30, 72$).

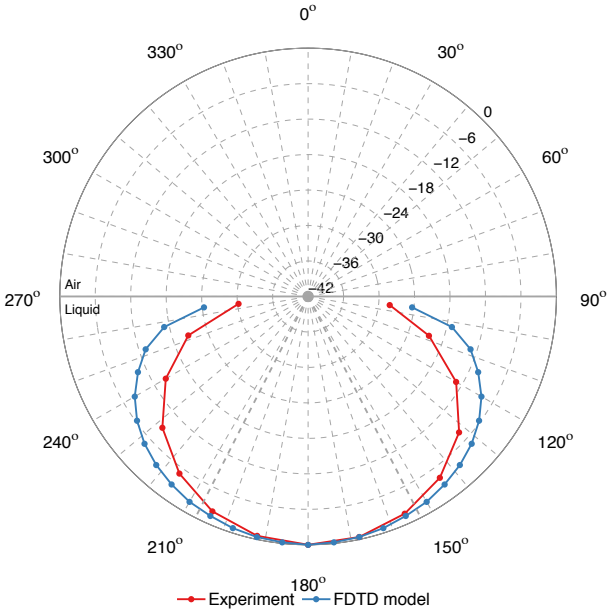

Fig. 5. Experimental and modelled 'received energy' H-plane patterns in emulsion of permittivity $\epsilon_r = 5$.

solid grey line in the plots represents the boundary between air and the dielectric environment and, where appropriate, dotted grey lines indicate the critical angle window. Table I

TABLE I
RADIATION PATTERN PARAMETERS

ϵ_r	θ_c (°)	λ (m)	R (m)	r/λ
5	27	0.089	0.081	1.23
10	18	0.063	0.114	1.74
30	11	0.037	0.197	3.02
72	7	0.024	0.306	4.67

presents electromagnetic wave properties for the dielectric environments that were used in the experiments. The critical angle in the dielectric environment is given by θ_c, while r is the observation distance (0.11 m). The observation distance was limited by the physical constraints of the apparatus, and the need to be able to clearly identify the wavelet reflected from the rebar in all responses. Despite this, target detection at a distance of 0.11 m is still a valid application of such a high-frequency antenna. The r/λ ratio is the observation distance in wavelengths. R is theoretical boundary between the radiating near-field and far-field of the antenna [21], calculated using Eq. (2).

$$R = \frac{2D^2}{\lambda} \tag{2}$$

D is the largest dimension of the antenna (0.060 m), and λ is the wavelength in the medium, calculated using the centre frequency of the antenna (1.5 GHz).

Fig. 4 presents the H-plane patterns from the experimental data in the different dielectric environments. As expected all of the patterns show a broad main lobe with maximum power directly under the antenna (180°). As the permittivity of the dielectric environment increases the main lobe becomes narrower, e.g. in the tap water ($\epsilon_r = 72$) it is approximately 6 dB narrower than the lowest permittivity emulsion ($\epsilon_r = 5$) at angles beyond 150°,210°. It can be observed that despite T_x and R_x elements of the antenna being offset from each another, the H-plane pattern is symmetric about the vertical axis (0°,180°). This is because the path distance (from T_x to the rebar target to R_x) is the same for radial positions on either side of the vertical axis.

Figs. 5–8 present comparisons of the H-plane patterns from experimental data with the FDTD numerical model in the different dielectric environments. In Fig. 5 the observation distance of 0.11 m (1.23 λ) from the antenna is theoretically in the far-field ($R = 0.081\ m$). However, this boundary definition is fuzzy when applied to a impulse-driven UWB antenna. A recent study [20] suggested the far-field does not begin until 10λ from the antenna. In Fig. 5 both experimental and modelled patterns show a broad main lobe with maximum power directly under the antenna (180°), decreasing to half-power (-3 dB) just beyond the critical angle (153°, 207°). The FDTD model begins to over-predict the power of the experimental pattern beyond the critical angle, with a maximum discrepancy of 6 dB at around 120° and 240°.

In Fig. 6 the behaviour is similar except that half-power now occurs beyond, rather that at, the critical angle (162°, 198°) at 145° and 215°. In Fig. 7 the correlation between the experimental and modelled results is improved but there are still differences of 3 dB at shallow angles. Fig. 8 presents the results from tap water. The main lobe has narrowed and

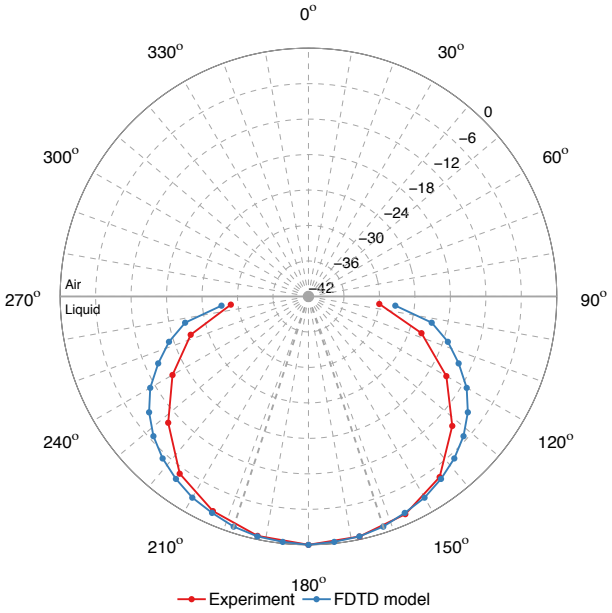

Fig. 6. Experimental and modelled 'received energy' H-plane patterns in emulsion of permittivity $\epsilon_r = 10$.

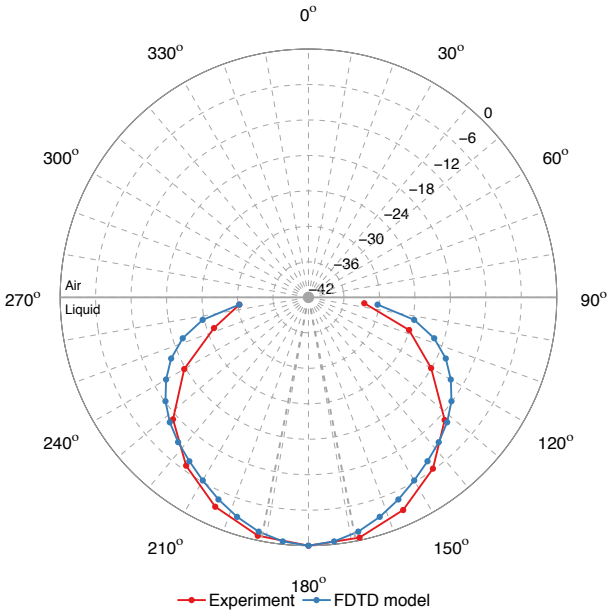

Fig. 7. Experimental and modelled 'received energy' H-plane patterns in emulsion of permittivity $\epsilon_r = 30$.

side lobes are beginning to appear in both experimental and modelled patterns at around 135° and 225°. It is also around these angles the modelled pattern deviates from the measured pattern, over-predicting by up to 6 dB.

V. Conclusion

The investigation of radiation characteristics of an antenna makes it possible to develop a better understanding of how

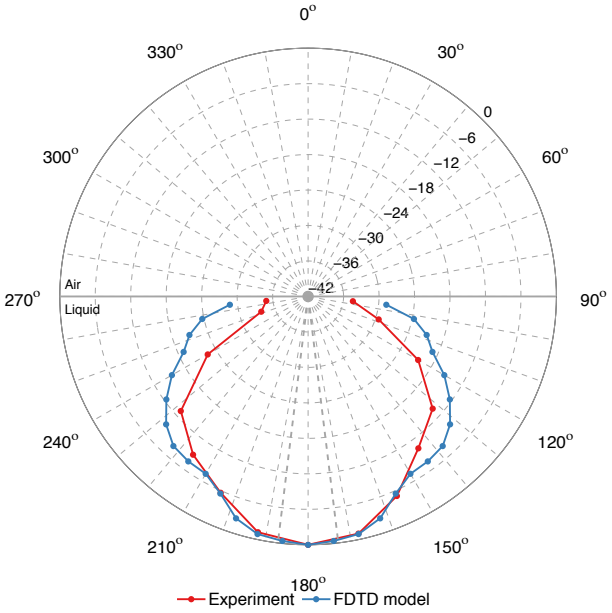

Fig. 8. Experimental and modelled 'received energy' H-plane patterns in water of permittivity $\epsilon_r = 72$.

the antenna radiates and receives energy. This is important for GPR as, for example, it can lead to a better understanding of the spatial resolution of a GPR antenna and how it can discriminate between closely spaced targets.

Physical measurements of the sensitivity of a high-frequency GPR antenna have been made in lossy dielectrics with a range of different permittivities. These measurements were made in the near-field of the antenna at a observation distance that shallow targets may typically be detected. For the range of permittivities studied, the H-plane patterns exhibit broad main lobes, but without the nulls present at the critical angles in analytical far-field patterns. Comparison between these measured patterns and those generated from a 3D FDTD model is generally good, but differences exist particularly at shallow angles.

Acknowledgment

This work benefited from networking activities carried out within the EU funded COST Action TU1208 "Civil Engineering Applications of Ground Penetrating Radar."

This work made use of the facilities of HECToR, the UK's national high-performance computing service, which is provided by UoE HPCx Ltd at the University of Edinburgh, Cray Inc and NAG Ltd, and funded by the Office of Science and Technology through EPSRC's High End Computing Programme.

References

[1] R. W. King, *Theory of Linear Antennas with Charts and Tables for Practical Applications*, 1956.

[2] N. Engheta, C. Papas, and C. Elachi, "Radiation patterns of interfacial dipole antennas," *Radio Science*, vol. 17, pp. 1557–1566, 1982.

[3] G. Smith, "Directive properties of antennas for transmission into a material half-space," *IEEE Transactions on Antennas and Propagation*, vol. 32, no. 3, pp. 232–246, 1984.
[4] S. Millard, A. Shaari, and J. Bungey, "Field pattern characteristics of GPR antennas," *NDT and E International*, vol. 35, no. 7, pp. 473–482, 2002.
[5] G. Klysz, X. Ferrieres, J. Balayssac, and S. Laurens, "Simulation of direct wave propagation by numerical FDTD for a GPR coupled antenna," *NDT and E International*, vol. 39, no. 4, pp. 338–347, 2006.
[6] V. Pérez-Gracia, D. Di Capua, R. González-Drigo, and L. Pujades, "Laboratory characterization of a GPR antenna for high-resolution testing: Radiation pattern and vertical resolution," *NDT and E International*, 2009.
[7] A. Annan, W. Waller, D. Strangway, J. Rossiter, J. Redman, and R. Watts, "The electromagnetic response of a low-loss, 2-layer, dielectric earth for horizontal electric dipole excitation," *Geophysics*, vol. 40, pp. 285–298, 1975.
[8] S. Arcone, "Numerical studies of the radiation patterns of resistively loaded dipoles," *Journal of Applied Geophysics*, vol. 33, pp. 39–52, 1995.
[9] S. Radzevicius, C. Chen, L. Peters, and J. Daniels, "Near-field dipole radiation dynamics through FDTD modeling," *Journal of Applied Geophysics*, vol. 52, no. 2-3, pp. 75–91, 2003.
[10] C. Warren and A. Giannopoulos, "Creating FDTD models of commercial GPR antennas using Taguchi's optimisation method," *Geophysics*, vol. 76, no. 37, 2011.
[11] L. Gurel and U. Oguz, "Three-dimensional FDTD modeling of a ground-penetrating radar," *IEEE Transactions on Geoscience and Remote Sensing*, vol. 38, no. 4, pp. 1513–1521, 2000.
[12] K.-H. Lee, C.-C. Chen, F. Teixeira, and R. Lee, "Modeling and investigation of a geometrically complex UWB GPR antenna using FDTD," *IEEE Transactions on Antennas and Propagation*, vol. 52, no. 8, pp. 1983–1991, 2004.
[13] Y. Nishioka, O. Maeshima, T. Uno, and S. Adachi, "FDTD analysis of resistor-loaded bow-tie antennas covered with ferrite-coated conducting cavity for subsurface radar," *IEEE Transactions on Antennas and Propagation*, vol. 47, no. 6, pp. 970–977, 1999.
[14] R. L. Roberts and J. J. Daniels, "Modeling near-field GPR in three dimensions using the FDTD method," *Geophysics*, vol. 62, no. 4, pp. 1114–1126, 1997.
[15] A. Giannopoulos, *GprMax - FDTD based GPR simulation software*, 2005.
[16] L. Galagedara, J. Redman, G. Parkin, A. Annan, and A. Endres, "Numerical modeling of GPR to determine the direct ground wave sampling depth," *Vadose Zone Journal*, vol. 4, pp. 1096–1106, 2005.
[17] M. Jeannin, S. Garambois, C. Grégoire, and D. Jongmans, "Multiconfiguration GPR measurements for geometric fracture characterization in limestone cliffs (Alps)," *Geophysics*, vol. 71, p. B85, 2006.
[18] O. Lopera and N. Milisavljevic, "Prediction of the effects of soil and target properties on the antipersonnel landmine detection performance of ground-penetrating radar: A Colombian case study," *Journal of Applied Geophysics*, vol. 63, no. 1, pp. 13–23, 2007.
[19] F. Soldovieri, J. Hugenschmidt, R. Persico, and G. Leone, "A linear inverse scattering algorithm for realistic GPR applications," *Near Surface Geophysics*, vol. 5, no. 1, pp. 29–42, 2007.
[20] N. Diamanti and A. P. Annan, "Characterizing the energy distribution around gpr antennas," *Journal of Applied Geophysics*, vol. 99, pp. 83–90, 2013.
[21] J. Kraus, *Electromagnetics*. WCB/McGraw-Hill, 1991.
[22] P. Debye, "Polare Molekeln," *Leipzig: Hirzel,— c1929*, 1929.